Wavelet-based threshold denoising for imaging hyperspectral data

Yang Hao[1,2], Zhang Dongyan[1,2,3*], Huang Linsheng[1,3], Zhao Jinling[1,3]

(1. *Key Laboratory of Agricultural Information Technology, Ministry of Agriculture, Beijing 100081, China*;
2. *Beijing Research Center for Information Technology in Agriculture, Beijing 100097, China*;
3. *College of Electronic and Information Engineering, Anhui University, Hefei 230601, China*)

Abstract: Imaging spectroradiometer is highly susceptible to noise. Accurately quantitative processing with higher quality is obligatory before any derivative analysis, especially for precision agricultural application. Using the self-developed Pushbroom Imaging Spectrometer (PIS), a wavelet-based threshold (WT) denoising method was proposed for the PIS imaging hyperspectral data. The WT with PIS was evaluated by comparing with other popular denoising methods in pixel scale and in regional scale. Furthermore, WT was validated by chlorophyll concentration retrieval based on red-edge position extraction. The result indicated that the determination coefficient R^2 of the chlorophyll concentration inversion model of winter wheat leaves was improved from 0.586 to 0.811. It showed that the developed denoising method allowed effective denoising while maintaining image quality, and presented significant advantages over conventional methods.

Keywords: wavelet, denoising, spectral domain, Pushbroom Imaging Spectrometer, red edge position
DOI: 10.3965/j.ijabe.20140703.005

Citation: Yang H, Zhang D Y, Huang L S, Zhao J L. Wavelet-based threshold denoising for imaging hyperspectral data. Int J Agric & Biol Eng, 2014; 7(3): 36－42.

1 Introduction

Hyperspectral images consist of spatial maps of intensity variations across a large number of spectral bands or wavelengths, integrating both spectroscopy and imaging techniques; alternatively, they can be thought of as a measurement of the spectrum of light transmitted or reflected from each spatial location in a scene. Due to its non-destructive and chemical-free advantages, currently imaging hyperspectral data is used in a variety of applications such as precision agriculture[1-4], environment monitoring[5], geological survey[6], food security[7-9] and medical diagnosis[10].

However, imaging spectroradiometer is highly susceptible to noise. The type of sensor is incapable of capturing a lot of energy due to their narrow bandwidth configuration, and cause self-generated noise inside the sensor. The recorded signal was influenced by complex environment including solar illumination and atmospheric absorption in the field. Most applications based on hyperspectral imagery data will be disturbed by the existing noise. Therefore, as a fundamental preprocessing, noise removal is an essential step before any further application.

Great efforts have been made to develop noise reduction techniques by signal processing community over the past several decades. As shown in the previous study[11], diffusion-weighted images can be denoised effectively through sparse dictionary learning constrained by the physical properties of the signal. Luo et al.[12] proposed an approach to medical image denoising based on a reconstruction-average mechanism. A multi-scale sparsity based tomographic denoising method was

Received date: 2014-01-16 **Accepted date:** 2014-05-24
Biographies: Yang Hao, PhD candidate, research interests: Agricultural information technology. Email: yangh@nercita.org.cn. **Huang Linsheng,** PhD, research interests: Agricultural information technology. Email: linsheng0808@163.com. **Zhao Jinling,** PhD, research interests: Agricultural information technology. Email: aling0123@163.com.
***Corresponding author: Zhang Dongyan,** PhD, Asistant Professor, research interests: Agricultural information technology. Address: College of Electronic and Information Engineering, Anhui University, NO.111, Jiulong Road, Hefei, China. Email: zhangdy@nercita.org.cn.

developed for optical coherence tomography images by Fang et al[13]. Mohanet et al.[14] used nonlocal neutrosophic set approach of Wiener filtering for magnetic resonance images. Wang et al.[15] proposed a modified illumination model for image deblurring and denoising problems. Perceptual frequency weighting filter is incorporated into Wiener filter to improve speech enhancement algorithms[16]. Despite diverse techniques aimed at different applications, there is no universal denoising method for all data since different signals have their own properties. In comparison to the above-mentioned methods which based on spatial domain or frequency domain, the method required in agriculture application of remote sensing pays main attention in spectral domain. Liu et al[17] and Li et al[18] used combination of wavelet package transformation and other filters for infrared spectrum. Axell et al[19] proposed a Bayesian approach for spectrum sensing denoising; Lin et al.[20] applied wavelet-based denoising for near infrared spectral data. These methods emphasized noisy portions of the spectrum where SNR (Singal-Noise-Ratio) was high and attenuated portions of the spectrum where the SNR was low. However, these methods were designed just for spectrum data (in one dimension) instead of for hyperspectral imaging data (in spectral and spatial dimension). More importantly, they were validated just by simulated data not actual data.

In 2010, a new field-based pushbroom imaging spectrometer (PIS) was developed by Zhang et al.[21]. The obtained hyperspectral images produce notable noise at both spatial dimension and spectrum dimension. The PIS is specially designed for precision agriculture application, such as vegetation nutrition diagnosis and nitrogen content retrieval quantitatively, which is very sensitive to denoising effect. It brings great challenge because the noise should be eliminated in high quality, and in the meanwhile the details should be preserved.

Therefore, the goal of the study is to develop an optimal denoising method suitable for PIS. Specially, the objectives are to: 1) evaluate the capacity of wavelet-based threshold denoising method for hyperspectral imagery data from PIS, when compared with other denoising methods; 2) validate the method by actual application, when crop leaf chlorophyll concentration was retrieved based on the denoised PIS data.

2 Materials and methods

2.1 Data collection

In the study, experimental data were collected in the key scientific observation station of precision agriculture and ecological environment located on Xiaotangshan town, Changping District of Beijing, China (40°11′16″ N, 116°27′03″ E). The cultivar of winter wheat, Jing 411 was selected as the research material and planted on September 30th, 2010. When the winter wheat was at the jointing stage, the hyperspectral data of 30 leaves were collected by PIS in the field on a sunny and breezy day. In the field the sample leaves were quickly picked and placed flat on a black, non-reflective cloth, and the corresponding spectra were measured at a distance of 120 cm from the lens of PIS to the sample leaf from 10:30 am to 15:30 pm during the day. After PIS data measurements were completed, all relative chlorophyll contents of the leaves were also measured by a SPAD-502 meter (Konica Minolta, Tokyo, Japan) for agricultural quantitative analysis.

Before the data acquisition of PIS, laboratory calibration was carried out to determine the location of the wavelengths, spectral response function, radiation accuracy, and spatial displacement. The specification parameters of PIS are spectral resolution closes 2 nm and spectral interval is 0.7 nm in the wavelength range from 400 to 1 000 nm. The field of view includes two types, which are 16 ° and 23 °, respectively, and the former was used to collect data in the study.

2.2 Data processing

Hyperspectral imagery can be viewed as a three-dimensional data cube which is constituted by a two-dimensional image and a one-dimensional spectrum. The two-dimensional image describes the target's spatial information feature while the one-dimensional spectrum information reveals the spectral profile feature of every pixel in the image. For every pixel in the image acquired by PIS, a sequence of digital number (DN) was obtained with a 0.7 nm spectrum interval.

Instrument calibration was performed firstly so that the DN values could be transformed into the relative reflectance. In the calibration, a linear empirical method was adopted:

$$X_i = A_i \times DN + B_i \quad (1)$$

In Equation (1), the coefficients A_i and B_i are calculated using the least squares method, and then the reflectance X_i is determined, in which, i is the index of any wavelength.

2.3 Denoising approaches

For a more accurate inversion of crop biochemical parameters, hyperspecral imagery data should be denoised for improving accuracy. In the study, a wavelet transform (WT) method was explored to remove the noise of the PIS imagery data, and some traditional denoising methods such as the Savitzky-Golay (SG) filter[22], moving average (MA)[23], and median filter (MF)[24] were also applied for purposes of comparison.

2.3.1 Wavelet transforms method

Among the numerous noise reduction techniques that were developed over the past several decades, wavelet-based threshold method has been one of the most successfully ones. Since its advent, WT has been utilized to remove noise in many different types of signals. WT transforms and zeros the coefficients below a certain threshold value, which is known as hard threshold, and then the noise coefficients would have significantly lower amplitude than the coefficients corresponding to the specific features. In addition, the coefficients remaining after the threshold operation could be reduced by the threshold value as well, which is known as soft threshold. In this study, the threshold-based wavelet denoising algorithm will include following three steps.

1) The discrete WT is carried out on the data sequence $f(t)$ after the wavelet filter and the numbers of decomposition layers are selected:

$$Y(d) = Y(f) + Y(z) \quad (2)$$

In Equation (2), $Y(d)$, $Y(f)$ and $Y(z)$ are the high-frequency WT components of the noisy data, truth data, and pure noise data, respectively.

2) A threshold is chosen for every level of the high-frequency coefficient and the WT coefficient $\hat{Y}(f)$ is estimated from the threshold. The soft threshold and hard threshold can be applied in Equations (3) and (4), in which T was the threshold.

For the soft threshold:

$$\hat{Y}(f) = \begin{cases} sgn(Y(d))(Y(d) - T) & |Y(d)| \geq T \\ 0 & |Y(d)| < T \end{cases} \quad (3)$$

For the hard threshold:

$$\hat{Y}(f) = \begin{cases} Y(d) & |Y(d)| \geq T \\ 0 & |Y(d)| < T \end{cases} \quad (4)$$

3) Wavelet reconstruction $\hat{Y}(f)$ was conducted to obtain an estimate of $\hat{Y}(t)$:

$$\hat{Y}(t) = \omega^{-1}\hat{Y}(f) \quad (5)$$

In Equation (5), ω^{-1} was the operator of wavelet inverse transformation.

It should be noted that the WT filter method is based on the choice of the threshold scheme. Usually, there are four schemes: Rigrsure, Sqtwolog, Heursure, and Minimaxi. While Rigrsure selects an adaptive threshold based on the Stein unbiased likelihood principle, Sqtwolog adopts a fixed threshold $\sqrt{2 \times \log(length(x))}$. Heursure is a mixture of these two schemes, while Minimaxi selects the mean square extreme error under non-ideal circumstances as the threshold.

Therefore, the effect of wavelet threshold method was influenced by many issues such as the choice of wavelet, the choice of decomposition level, threshold selection, and the choice of thresholding functions.

2.3.2 SG, MA and MF

SG filtering is based on least squares polynomial smoothing. It finds a smoothed value for each point in the spectrum of a subset of data within a slide window. The window contains the points to be smoothed in the centre position of the window as well as several of its neighbors. Only the central point is smoothed for each window position, although all the data within the window are used to perform the least squares fit. Other points are smoothed by moving the window across the spectrum point by point, performing a least squares approximation to the windowed data at each location.

The MA approach regards the average spectral value of all points within a specified window as the new value

of the middle point of the window. The method is solely based on linear calculations and has only one critical parameter, which is the filter window size. The MF method is similar to MA but the median value instead of the average value was used.

2.3.3 Smoothing index

A smoothing index (SI) in the study was designed to evaluate the denoising effect quantitatively. The expression formula was displayed as in Equation (6).

$$SI = \frac{\sum_{i=1}^{n} | \hat{\rho}_{i+1} - \hat{\rho}_i |}{\sum_{i=1}^{n} | \rho_{i+1} - \rho_i |} \quad (6)$$

In Equation (6), $\hat{\rho}$ and ρ represent the denoised spectrum and original spectrum, respectively, n means the number of wavebands, and SI reflects the curve smoothness. When SI value is smaller, the denoised spectrum is smoother.

3 Results and analysis

3.1 Denoising effect at different noise levels

As the blue curve in Figure 1, the reflectance spectrum of a single pixel was presented. The signal was contaminated by server noise in the wavelength range from 450 nm to 950 nm. Subsequently, much noise was filtered out after WT was applied, and a smooth curve (the red in Figure 1) which also preserved the spectrum shape was obtained.

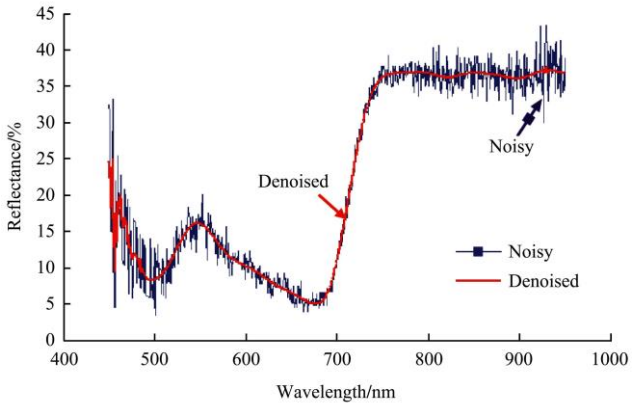

Figure 1 Results of WT for the single-pixel case

In fact, the spectrum noise can be reduced by exploiting the spatial correlation in the two-dimensional image which exists in the adjacent pixels. Hence, a region of interest in an image can be selected and an average reflectance in this region can be obtained for every band. For the multi-pixel case, a spectral curve with less noise was shown as blue curve in Figure 2. Even so further application of this noisy curve could have problematic in quantitative inversion of crop parameter. Therefore, WT was also applied on this less noisy spectrum. The denoised red curve in Figure 2 showed that the noise was removed effectively and the shape of the spectral curve was maintained in general.

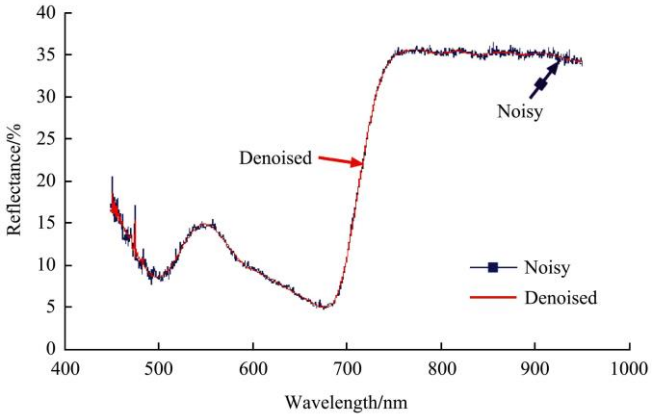

Figure 2 Results of WT for the multi-pixel case

It should be noted that the same WT parameters set was used at different noise levels (single-pixel and multi-pixel). Sqtwolog, soft threshold, and hierarchy threshold scheme were selected in wavelet transform filter (decomposition layers = 5, wavelet radix = ‘symlets20’). With these parameters WT was fairly consistent in noise reduction at different noise levels.

From Figures 1 and 2, it was found that the reflectance curves were abnormal at wavelengths of 450-480 nm, as they were higher than the normal value. This phenomenon was more serious with the decrease of the wavelength. In this wavelength range, the spectrum had high disturbance, and even after WT, noise still existed in both single-pixel and multi-pixel case. The problem may come from the instrument itself or reflectance calibration. Therefore, only the wavelength range greater than 480 nm was considered in the further analysis.

Therefore, the results presented the capability of wavelet-based denoising method both in pixel scale and in regional scale. It was worthy of noting that study in single pixel is usually used for instrument performance evaluation and calibration while study in region is more used for quantitative retrieval in agriculture.

3.2 Comparison with SG, MA and MF

For the purpose of comparison with the WT method, the SG, MA, and MF methods were also used for noise reduction. To present more details, a noisy spectrum and a spectrum denoised by WT and SG only within the range of 670-970 nm were shown in Figure 3. Visually, it was clear that the spectrum denoised by WT was smoother while much jaggedness were remained in the one denoised by SG. However, usually it was hard to distinguish the difference visually. Here we used the SI to assess the affection of noise reduction in different denoised methods. Table 1 listed the SI values of the four methods. We defined the SI of noisy spectrum as 1, if SI value became littler; it meant denoised effect was better. The SIs of the four methods in Table 1 were 0.09 (WT), 0.14 (SG), 0.13 (MA), 0.18 (MF), respectively, the order of denoised effect was WT>MA> SG>MF. This indicated that WT had the best performance regard to smoothing ability.

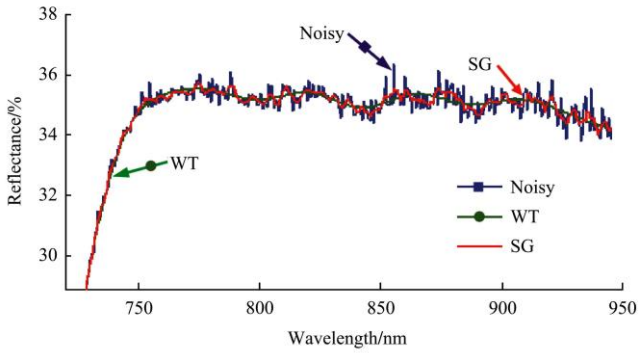

Figure 3 Results of the WT and SG denoising

Table 1 SIs of the four methods

Original	WT	SG	MA	MF
1.00	0.09	0.14	0.13	0.18

Note: WT, wavelet transform; SG, Savitzky-Golay; MA, moving average; MF, median filter.

3.3 Application analysis

Use of noise reduction methods made the spectral curves smoother, but may cause some loss of information or change certain subtle feature of original spectrum simultaneously, which will produce incorrect results in subsequent analyses. Therefore, besides smoothing ability, an excellent noise reduction technique should maintain the curve characteristics, which were reflected by the curve shape or location of characteristics such as peaks, valleys, inflection points, and so on.

Red edge, which reflects variations in the chlorophyll content and biomass of vegetation, is a very important feature to invert biochemical and biophysical parameters of vegetation using hyperspectral remote sensing. The position of the red edge and the chlorophyll content are of great relevance[25]. When the chlorophyll content becomes high, the red edge moves towards the long wavelength direction. To evaluate the feature-conservation ability of the WT method, red edge position (REP) [26] was extracted from the noisy spectrum and the denoised spectrum, respectively, and then analyzed the relationship between REP and the chlorophyll content of the corresponding leaf (Figure 4). The high correlation coefficient (R^2) indicated a strong feature-conservation ability and better denoising effect. The first order derivative was used for red edge position extraction. The relative chlorophyll contents were measured by SPAD-502.

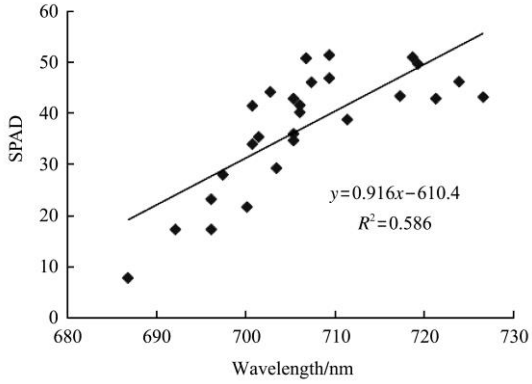

(a)

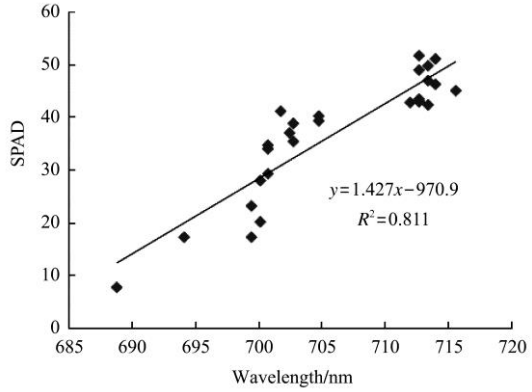

(b)

Figure 4 (a) Relationship between SPAD and REP of noisy spectra; (b) Relationship between SPAD and REP of denoised spectra

After removing three abnormal samples from the 30 leaf samples collected, the linear regression models of the

27 samples were presented in Figure 4. In Figure 4(a), the determination coefficient R^2 was 0.586 between SPAD and REP extracted from the noisy spectra, while in Figure 4(b) R^2 reached 0.811 between SPAD and REP extracted from the WT-based denoised spectra. Thus, after noise reduction by using WT, the coefficient of correlation was obviously improved. However, there was significant difference for scattered points in Figure 4. The former variation regions of REP were from 688 nm to 728 nm, and almost focused on 700-710 nm. The latter change ranges were from 689 nm to 716 nm, and almost concentrated on 700-705 nm. Although the determination coefficient had the larger improvement before and after WT-based denoising, why the variance of scattered points had obviously changed, which can be explained by combining Figure 1 with Figure 2. In the study, REP was calculated as maximum value of first order derivative, and especially flexible altered in spectral interval of 0.7 nm after noisy disturbance. This was a very important reason that we must explore suitable denoised way to decrease the randomness of hyperspectral data.

From the above, combination spectral curve (Figures 1 and 2) with analysis result of inversion model (Figure 4), it can be concluded that the WT maintained the spectral characteristics efficiently.

4 Conclusions and discussion

This study presented an approach to remove the noise on hyperspectral imagery data collected by PIS. With the aim of carrying out quantitative inversion of crop biochemical parameters, the WT method was developed, and commonly used denoising methods such as the SG method, MA method, and MF method were compared. A SI index was designed to evaluate the denoising effect. For the SI queuing, it was concluded that WT>MA>SG>MF, which indicated that the WT method had the best smoothness. Meanwhile, WT showed its consistency when applied to a noisy spectrum at different noise levels. Furthermore, the REP was extracted from the denoised spectrum and its relationship with the chlorophyll content was analyzed. The R^2 of WT-based denoised reached 0.811, which was better than that of noisy spectra (R^2=0.586). The improvement in the application revealed that WT had fine feature-conservation ability.

However, the research results still have obvious shortages that need deeply exploration and perfection. In the study, we focused on spectral denoising of leaf hyperspectral image. Through comparing the traditional methods, the proposed MT was the best, the way whether adapted for other data such as crop canopy, different vegetation leaf and so on; this needs to design more experiments to validate. Moreover, we utilized the model based-red edge position to assess the feature-conservation effect of WT denoising, the result displayed that REP was an effective method to evaluate feature-conservation of denoised spectra[26]. However, this study was only a simple validation and needed multi-resource data to improve the WT-based denoised method. Besides, the data from PIS owned the advantage image and spectra as one; we should also explore certain imagery analysis method to promote better to utilize spectral information.

Acknowledgements

This study was financially supported by the Agricultural Outstanding Talent Research Fund and Open Fund of Key Laboratory of Agricultural Information Technology, Ministry of Agriculture (2012007), National Natural Science Foundation of China (41301471), Anhui Provincial Natural Science Foundation (1308085QC58) and Open Fund of State Key Laboratory of Remote Sensing Science (OFSLRSS201319). We are grateful to the reviewers for their helpful suggestions on the manuscript.

[References]

[1] Mulla D J. Twenty five years of remote sensing in precision agriculture: Key advances and remaining knowledge gaps. Biosystems Engineering, 2013; 114(4): 358－371.

[2] Lelong C C D, Pinet P C, Poilvé H. Hyperspectral imaging and stress mapping in agriculture: A case study on wheat in Beauce (France). Remote Sensing of Environment, 1998; 66(2): 179－191.

[3] Huang W, Lamb D W, Liu Z, Zhang Y, Liu L, Wang J. Identification of yellow rust in wheat using in-situ spectral

reflectance measurements and airborne hyperspectral imaging. Precision Agriculture, 2007; 8(4-5): 187－197.

[4] Mariotto I, Thenkabail P S, Huete A, Slonecker E T, Platonov A. Hyperspectral versus multispectral crop-productivity modeling and type discrimination for the HyspIRI mission. Remote Sensing of Environment, 2013; 139: 291－305.

[5] Schaepman M E, Ustin S L, Plaza A J, Painter T H, Verrelst J, Liang S. Earth system science related imaging spectroscopy—An assessment. Remote Sensing of Environment, 2009; 113: S123－S137.

[6] Haest M, Cudahy T, Rodger A, Laukamp C, Martens E, Caccetta M. Unmixing the effects of vegetation in airborne hyperspectral mineral maps over the Rocklea Dome iron-rich palaeochannel system (Western Australia). Remote Sensing of Environment, 2013; 129: 17－31.

[7] Guo Z M, Huang W Q, Chen L P, Peng Y K, Wang X. Shortwave infrared hyperspectral imaging for detection of pH value in Fuji apple. International Journal of Agricultural and Biological Engineering, 2014; 7(2): 130－137.

[8] Kamruzzaman M, ElMasry G, Sun D W, Allen P. Application of NIR hyperspectral imaging for discrimination of lamb muscles. Journal of Food Engineering, 2011; 104(3): 332－340.

[9] ElMasry G, Sun D W, Allen P. Non-destructive determination of water-holding capacity in fresh beef by using NIR hyperspectral imaging. Food Research International, 2011; 44(9): 2624－2633.

[10] Martin M E, Wabuyele M B, Chen K, Kasili P, Panjehpour M, Phan M, et al. Development of an advanced hyperspectral imaging (HSI) system with applications for cancer detection. Annals of biomedical engineering, 2006; 34(6): 1061－1068.

[11] Gramfort, A, Poupon, C, Descoteaux, M. Denoising and fast diffusion imaging with physically constrained sparse dictionary learning. Medical Image Analysis, 2014; 18(1): 36－49.

[12] Luo J H, Zhu Y M. Denoising of medical images using a reconstruction-average mechanism. Digital Signal Processing, 2012; 22(2): 337－347.

[13] Fang L Y, Li S T, Nie Q, Izatt J A, Toth C A, Farsiu S. Sparsity based denoising of spectral domain optical coherence tomography images. Biomedical Optics Express, 2012; 3(5): 927－942.

[14] Mohan J, Krishnaveni V, Guo Y H. MRI denoising using nonlocal neutrosophic set approach of Wiener filtering. Biomedical Signal Processing and Control, 2013; 8(6): 779－791.

[15] Wang S, Huang T Z, Liu J, Lv X G. An alternating iterative algorithm for image deblurring and denoising problems. Communications in Nonlinear Science and Numerical Simulation, 2014; 19(3): 617－626.

[16] Jahangir A L A M, Chowdhury F A, Fasiul A L A M. Wiener denoising based on perceptual frequency weighting and noise spectrum shaping. IU-Journal of Electrical & Electronics Engineering, 2013; 13(1): 1589－1595.

[17] Liu Y P, Gao G R, Gong N, Huang R H. Infrared spectrum denoising with combination of lifting wavelet domain thresholding and median filtering. Spectroscopy and Spectral Analysis, 2012; 32(8): 2085－2088.

[18] Li H, Lin Q Z, Wang Q J, Liu Q J, Wu Y Z. Research on spectrum denoising methods based on the combination of wavelet package transformation and mathematical morphology. Spectroscopy and Spectral Analysis, 2010; 30(3): 644－648.

[19] Axell E and Larsson E G. A bayesian approach to spectrum sensing, denoising and anomaly detection, proceedings of the 34th IEEE International Conference on Acoustics, Speech and Signal Processing (ICASSP'09), 2009; 2333－2336.

[20] Lin X M, Wang J, Yao Q H. Wavelet analysis of near infrared spectral data in the application of denoising. Applied Mechanics and Materials, 2011; 1358: 48－49.

[21] Zhang D Y, Song X Y, Ma Z H, Yang G J, Huang W J, Wang J H. Assessment of the developed Pushbroom Imaging Spectrometer in single leaf scale. Scientia Agricultura Sinica, 2010; 43(11): 2239－2245.

[22] Chen J, Jönsson P, Tamura M, Gu Z H, Matsushita B, Eklundh L. A simple method for reconstructing a high-quality NDVI time-series data set based on the Savitzky–Golay filter. Remote sensing of Environment, 2004; 91(3): 332－344.

[23] Said S E, Dickey D A. Testing for unit roots in autoregressive-moving average models of unknown order. Biometrika, 1984; 71(3): 599－607.

[24] Brownrigg D R K. The weighted median filter. Communications of the ACM, 1984; 27(8): 807－818.

[25] David L D. and Iain M J. Ideal denoising in an orthonormal basis chosen from a library of bases. Academic Science Series (I), 1994; 319: 1317－1322.

[26] Cho M A, Skidmore A K. A new technique for extracting the red edge position from hyperspectral data: The linear extrapolation method. Remote Sensing of Environment. 2006; 101: 181－193.